Journal of Saudi Chemical Society (2016) **xxx**, xxx–xxx

King Saud University

Journal of Saudi Chemical Society

www.ksu.edu.sa
www.sciencedirect.com

ORIGINAL ARTICLE

Structural, impedance and Mössbauer studies of magnesium ferrite synthesized via sol–gel auto-combustion process

Shahid Khan Durrani [a], **Sumaira Naz** [a,b,*], **Mazhar Mehmood** [b], **Muhammad Nadeem** [c], **Muhammad Siddique** [c]

[a] *Materials Division, Directorate of Technology, Pakistan Institute of Nuclear Science and Technology (PINSTECH), Nilore, Islamabad, Pakistan*
[b] *National Centre for Nanotechnology, Department of Metallurgy and Materials Engineering, Pakistan Institute of Engineering and Applied Sciences (PIEAS), Islamabad 45650, Pakistan*
[c] *Physics Division, Directorate of Science, Pakistan Institute of Nuclear Science and Technology (PINSTECH), Nilore, Islamabad, Pakistan*

Received 5 November 2015; revised 19 December 2015; accepted 20 December 2015

KEYWORDS

Sol–gel auto-combustion;
Magnesium ferrite;
X-ray diffraction;
SEM;
Mössbauer spectroscopy;
Impedance spectroscopy

Abstract Crystalline magnesium ferrite ($MgFe_2O_4$) spinel oxide powder was synthesized by nitrate–citrate sol–gel auto-combustion process with stoichiometric composition of metal nitrate salts, urea and citric acid. The study was focused on the modification of synthesis conditions and effect of these modified conditions on the structural and electrical properties of synthesized $MgFe_2O_4$ ceramic materials. Phase composition, crystallinity, structure and surface morphology were studied by X-ray diffraction, FTIR and SEM. Pure single phase $MgFe_2O_4$ spinel ferrite was obtained after calcination at 850 °C. Rietveld refinement of XRD result confirmed the single cubic phase spinel oxide with the lattice constant of $a = 8.3931$ Å and Fd3m symmetry. UV–visible absorption study of calcined powder revealed an optical band gap of 2.17 eV. SEM images of sintered specimens (1050–1450 °C) showed that the grain size increased with the increase in sintering temperature. From the impedance results of the sintered $MgFe_2O_4$ specimens, it was found that the resistance of grain, grain boundary and electrode effect decreased with an increase in sintering temperature and associated grain growth. In the intermediate frequency region lowering of impedance and dielectric values was observed due to the decrease in grain boundary areas. Mössbauer studies

* Corresponding author at: Materials Division, Directorate of Technology, Pakistan Institute of Nuclear Science and Technology (PINSTECH), Nilore, Islamabad, Pakistan. Tel.: +92 51 9248840; fax: +92 51 9248808.
E-mail address: sumaira.chemist@gmail.com (S. Naz).
Peer review under responsibility of King Saud University.

Production and hosting by Elsevier

http://dx.doi.org/10.1016/j.jscs.2015.12.006

Please cite this article in press as: S.K. Durrani et al., Structural, impedance and Mössbauer studies of magnesium ferrite synthesized via sol–gel auto-combustion process, Journal of Saudi Chemical Society (2016), http://dx.doi.org/10.1016/j.jscs.2015.12.006

indicated that magnesium ferrite had a mixed spinel structure in calcined and sintered samples, however, the well refined single phase $MgFe_2O_4$ was observed due to well developed high crystalline structure at 1350 °C and 1450 °C.

1. Introduction

Crystalline ferrite magnetic materials could provide more advantages over the bulk ferrite materials with reminiscent change of physical properties such as extremely small size and increase in surface area to volume ratio [1]. Crystals of spinel ferrites, with general formula MFe_2O_4 (where M = Mg, Ni, Cu and Zn) are the most interesting class of magnetic materials due to their fascinating properties such as low melting point, high specific heat, large expansion coefficient and low magnetic transition temperature [2,3]. Because of these properties, ferrite materials are widely used in ferrofluid technology, information storage and magnetic pigments [4–6]. Mainly, due to their peculiar magnetic properties and ability to respond at the molecular level, they are used for biomedicine such as targeted drug delivery [7], diagnostics [8], and magnetic separation [9]. These materials are also being explored as contrast agents in magnetic resonance imaging (MRI) [10], thermo responsive drug carriers [11], as well as, in the thermal activation therapy of cancer [12]. The crystal structure of spinel ferrite compounds has a cubic close packing of O^{2-} ions linked with two sub-lattice sites namely tetrahedral (A-sites) and octahedral (B-sites) [13]. Magnesium ferrite ($MgFe_2O_4$) is an important magnetic oxide with cubic structure of normal spinel-type. It is a soft magnetic n-type semiconducting material with a band gap of 2.18 eV [14,15]. $MgFe_2O_4$ and allied compounds have found wide spread applications in microwave devices because of a low magnetic and dielectric loss [16]. It has also been utilized in high density recording media [17], heterogeneous catalysis [18], sensors [19,20], etc. $MgFe_2O_4$ is known for its good photoelectric effect [21–23] and as well as, is a promising candidate for local heating in human cancer therapy [24,25].

The synthesis of nanocrystalline spinel ferrites has been investigated extensively in recent years for their new and improved properties and their potential applications in high-quality filters, transformer cores, radio frequency circuits and rod antennas [26]. The methods of preparation play a very important role in determining the chemical, structural and magnetic properties of spinel ferrites. The micronsized ferrites are commonly prepared by ceramic technique like solid state method that involves high-temperature solid state reactions between the constituent oxides, carbonates or oxalates [27,28] resulting in nonuniformity of particle size and shape, formation of strongly bonded agglomerates, poor sintering behavior and reproducibility, imprecise control of cation stoichiometry and time consuming process. For crystallite ferrites, wet chemical techniques have been extensively recognized as an efficient approach for the synthesis of high surface area and homogenous magnetic spinel oxides at a low temperature and great attention has been given for the improvement of these fabrication methods [29]. In wet chemical process, the various methods have been used to produce crystalline magnesium ferrite such as coprecipitation [30], mechanochemical [31], microemulsion [32,33], sonochemical [34], sol–gel [35,36], sol-spray drying [37], solvothermal [38] and hydrothermal processes [39–45]. All these processes have their own advantages and disadvantages, depending on desired properties and applications. Recently, a simple and versatile sol–gel auto-combustion process has emerged as an important technique for the synthesis and processing of advanced ceramics (structural and functional), catalysts, composites and crystalline spinel oxide materials [46–48]. In sol–gel auto-combustion process, the exothermicity of the redox (reduction–oxidation or electron transfer) chemical reaction is used to produce useful materials with homogeneous mixing and good stoichiometric control. Sol–gel auto-combustion is an attractive method for the manufacturing of technologically useful materials at a low cost compared to conventional ceramic process [49,50].

The objective of present research work is to study the versatile and cost effective sol–gel auto-combustion process by the combination of urea-citrate-nitrate in order to obtain crystalline magnesium ferrite and investigate structural, electrical and Mössbauer properties after sintering at various temperatures using X-ray diffraction, SEM, UV–visible, FTIR, Mössbauer and impedance spectroscopic analysis.

2. Experimental

2.1. Materials

Starting materials used in the present study were magnesium nitrate ($Mg(NO_3)_2{\cdot}6H_2O$, Merck, 99%), ferric nitrate 9-hydrate ($Fe(NO_3)_3{\cdot}9H_2O$, Merck, 99.9%), urea ($CO(NH_2)_2$, Merck, 99.9%), citric acid ($C_6H_8O_7{\cdot}H_2O$, Merck 99.9%) and ammonium hydroxide (NH_4OH, Merck). All chemicals were of analytical reagent grade. Double-distilled water (DDW) with conductivity less than 5 $\mu S\,cm^{-1}$ (Iwaki WS-6 Water Still/Metrohm 712 Conductometer) was used in all the experiments.

2.2. Method

Crystalline magnesium iron ferrite powder was synthesized according to specified sol–gel auto-combustion processes [46–50] with modifications. In a typical process, known concentration of nitrate solutions were prepared by dissolving ferric nitrate and magnesium nitrate in double distilled water (DDW). These nitrate solutions were then mixed by volume according to specified proportions and appropriate amount of urea and citric acid was finally added in the mixed solution. The pH of the solution was adjusted in the range of 6–7. The solution was then heated at about 70 °C in a rotary evaporator (Heidolph Laborota 4001) for 4 h until a viscous sol (xerogel) was obtained. The xerogel was transferred into a ceramic

Please cite this article in press as: S.K. Durrani et al., Structural, impedance and Mössbauer studies of magnesium ferrite synthesized via sol–gel auto-combustion process, Journal of Saudi Chemical Society (2016), http://dx.doi.org/10.1016/j.jscs.2015.12.006

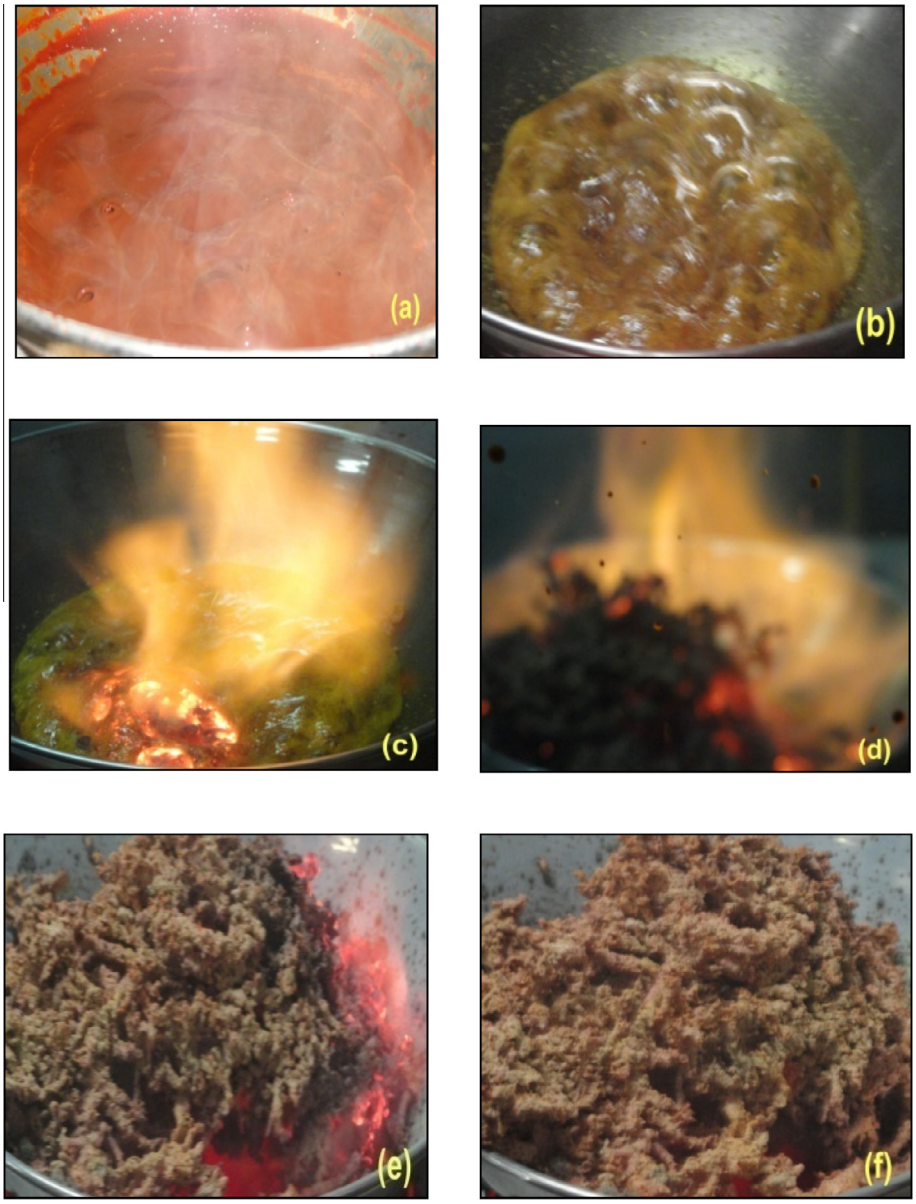

Figure 1 Sol–gel auto-combustion process for preparation of soft magnetic material ($MgFe_2O_4$): (a) sticky sol, (b) condense gel heated at 120 °C, (c) auto combustion started, (d) full combustion at 250 °C, (e) slow down combustion, and (f) foaming powder material of $MgFe_2O_4$.

bowel and was heated on a hot plate. The gel initially started swelling, producing foamy precursor and then a rapid and vigorous auto ignition took place for about a minute, completing the reaction. Typical images of a sample being prepared by auto-combustion method are shown in Fig.1. The resultant foaming powder was grounded and calcined at a prescribed temperature (550–850 °C) for 4 h. A fine powder with typical brown color of $MgFe_2O_4$ was obtained.

2.3. Pellets fabrication and sintering

The calcined powder was grounded in acetone medium for about 1 h using a ball mill, for deagglomeration. The fine powder was pressed uni-axially using a hydraulic press (Komage Germany) of load capacity of 5 t/in^2 (1 t/in^2 = 15.44 MPa) into 20 mm diameter pellets. The organic polymer polyvinyl alcohol (5 wt.% PVA) was used as the binder material. The green compacts were then sintered in a muffle furnace at different temperatures ranging from 1050 to 1450 °C for 4 h. Heating rate was maintained at 5 °C/min, while the cooling was performed in the furnace.

2.4. Characterization

Structural characterization (crystallinity and phase analysis) of synthesized products were conducted by X-ray diffraction using Rigaku Geiger flux instrument (Dmax-IIIA) with CuK_α radiation. The XRD data were collected in the 2θ range of 10–70° at a scan rate of 3°/min. A horizontal assembly dilatometer (NETZSCH 409) was used to study the shrinkage behavior.

Please cite this article in press as: S.K. Durrani et al., Structural, impedance and Mössbauer studies of magnesium ferrite synthesized via sol–gel auto-combustion process, Journal of Saudi Chemical Society (2016), http://dx.doi.org/10.1016/j.jscs.2015.12.006

Micro-structural features of synthesized materials and sintered pellets were observed by NOVA Nanosem-430 (FESEM). The elemental composition of synthesized oxide materials were measured by (EDX) attached with NOVA Nanosem-430 (FESEM). Densities of sintered polished pellets were measured by Archimedes method. Fourier transform infrared (FTIR) spectrum of magnesium ferrite powder specimen was recorded in the range of 400–4000 cm^{-1} on FTIR spectrometer (Thermo-Nicolet Avatar 370). The absorption spectrum of magnesium ferrite sample was recorded in transmission mode in the wavelength range of 200–900 nm on UV–visible spectrophotometer (Specord 205, Analtik Jena) by dispersing the powder particles uniformly in liquid paraffin. The $MgFe_2O_4$ calcined powder and sintered pellet specimens were sandwiched between two pieces of adhesive tape for Mössbauer effect measurements. The data collection was done at room temperature using a ^{57}Co source of 25 mCi strength, in transmission geometry. Mössbauer spectrometer was calibrated using a thin α-Fe foil. The Mössbauer data analysis was performed using a computer program MOS-90 assuming that the peaks are Lorentian in shape [51]. Impedance spectroscopy on sintered pellets of $MgFe_2O_4$ was performed in the frequency range of 1–10^7 Hz, using an Alpha-N Analyzer (Novocontrol). The contacts were made by silver paint on the opposite sides of the pellets. The ac signal amplitude was 0.2 V. WINDETA software was used for data acquisition and ZView software was used for the fitting of measured results.

3. Results and discussion

3.1. Structure characterization

Fig. 2 shows typical FTIR results for the sample calcined at 850 °C. The spectrum reveals absorption bands at around 535 cm^{-1} and 410 cm^{-1}. These bands are due to Fe^{3+}–O^{2-} stretching vibrations on tetrahedral and octahedral sites, respectively, characteristic of inverse spinel magnesium ferrites [52,53].

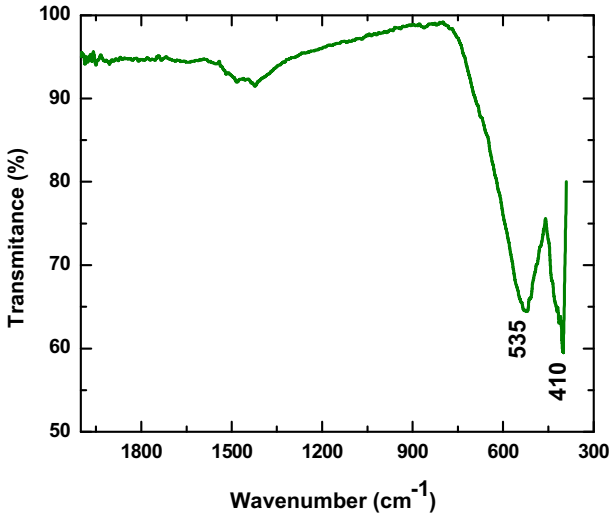

Figure 2 FTIR spectrum of $MgFe_2O_4$ powder calcined at 850 °C.

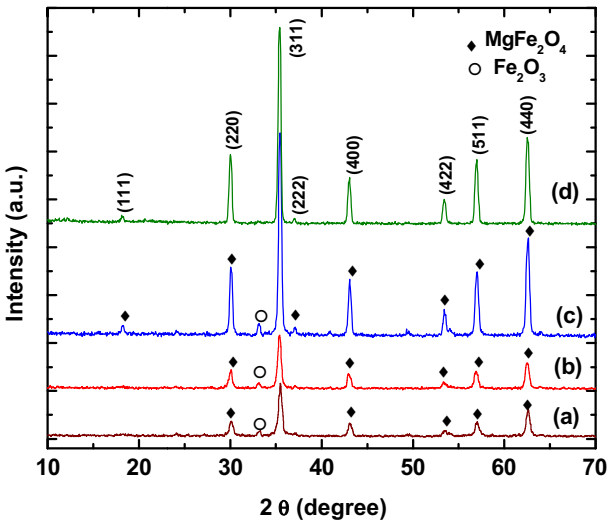

Figure 3 XRD patterns of $MgFe_2O_4$ power specimens calcined at: (a) 550 °C, (b) 650 °C, (c) 750 °C, and (d) 850 °C.

3.2. Phase analysis

Fig. 3 shows typical XRD patterns of the specimens calcined at 550 °C, 650 °C, 750 °C and 850 °C for 4 h in air. Up to 750 °C (Fig. 3a–c) minor impurity of Fe_2O_3 is seen. At 850 °C (Fig. 3d), Fe_2O_3 phase was completely eliminated and pure single phase of $MgFe_2O_4$ was achieved. The XRD patterns of the calcined samples (Fig. 3a–d) show that as the calcination temperature increases, peaks associated with $MgFe_2O_4$ become sharper and more intense indicating an improvement in crystalline quality with calcination temperature (and enhanced stoichiometry with dissolution of Fe_2O_3). All the sharp diffraction peaks were compared with standard diffraction lines of magnesium ferrite JCPDS Card No. 88-1943 [54]. The most prominent peak centered at $2\theta = 35.55°$ and corresponds to crystal plane (3 1 1) which is a characteristic peak of $MgFe_2O_4$ spinel structure. The other peaks are also assigned to spinel cubic structure (Fig. 3d) with Miller indices of (1 1 1), (2 2 0), (3 1 1), (2 2 2), (4 0 0), (4 2 2), (5 1 1) and (4 4 0).

The calcined powder specimens were pressed into pellets and sintered at 1050 °C, 1350 °C and 1450 °C for 4 h in air. Fig. 4 shows the refined XRD pattern of $MgFe_2O_4$ pellet specimen sintered at 1050 °C. All the peaks are well-defined indicating the high crystalline nature of the specimen. Rietveld refinement was carried out to verify the formation of spinel phase using the Rietica 77 software [55]. The Rietveld refined diffraction pattern (solid line) shown in Fig. 4 matches well with the measures pattern (dots). Rietveld refinement clearly indicates that $MgFe_2O_4$ crystallizes in the space group of Fd3m with lattice parameters of $a = b = c$ 8.3931 ± 0.01 Å, consistent well with the literature [54,56]. Rietveld refinement parameters are given in Table 1.

3.3. Dilatometric and sintering

The densification behavior of the compacts was examined by dilatometry. Fig. 5 illustrates a typical non-isothermal dilatometric curve of green compact of $MgFe_2O_4$ powder originally calcined at 850 °C. It may be noticed that any dimensional

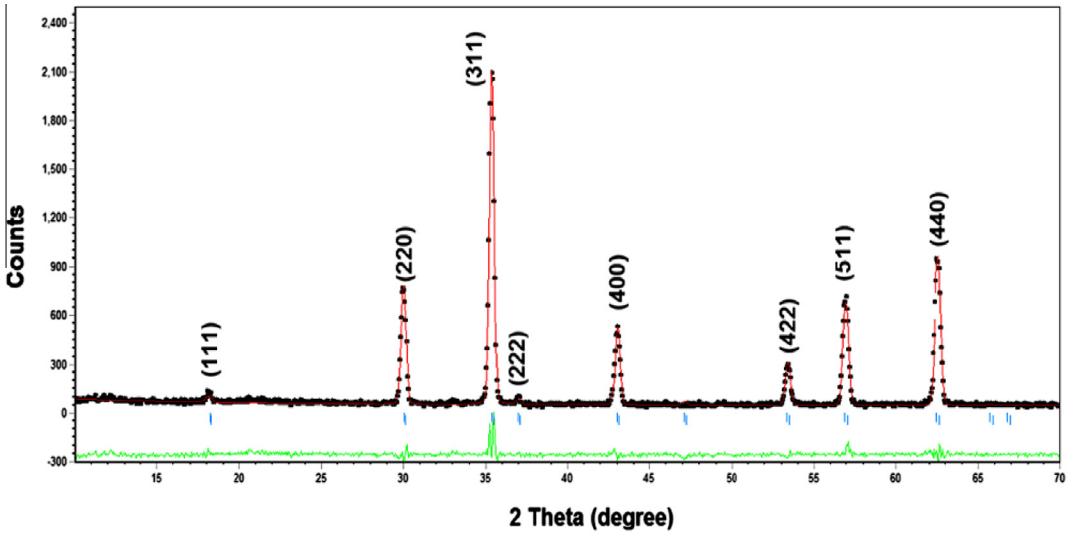

Figure 4 Rietveld refinement pattern of $MgFe_2O_4$ pellet sintered at 1050 °C.

Table 1 Structural parameters obtained from the Rietveld refinement of X-ray diffraction data of $MgFe_2O_4$ pellet sintered at 1050 °C.

Atoms	Wy/Position	*x*	*y*	*z*	B/A^2	*n*
Mg	8a	0.1250	0.1250	0.1250	1.0000	1.0000
Fe	16d	0.5000	0.5000	0.5000	1.0000	2.0000
O	32e	0.2560	0.2560	0.2560	0.0000	4.0000

Lattice parameters (Å)	Unit cell volume (Å^3)	Space group	R_p (%)	R_{wp} (%)	R_{exp} (%)	R_{bragg} (%)	GOF
8.39313	591.469	Fd3m	10.39	14.67	10.65	5.17	1.896

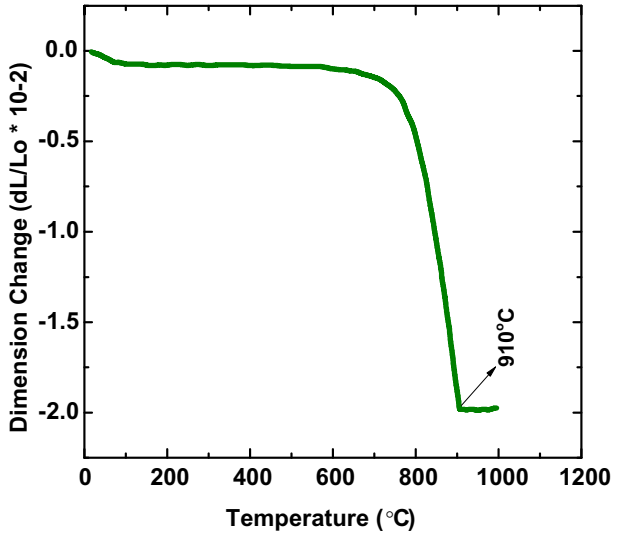

Figure 5 Thermodilatometric curve of green compact (pellet) of $MgFe_2O_4$ powder calcined at 850 °C.

change is not seen up to a temperature of 600 °C, above which pronounced contraction is observed particularly at around 900 °C.

3.4. Microstructure

In order to study the effect of sintering temperature on the morphology of $MgFe_2O_4$ ceramic materials, scanning electron microscopy was carried out. The microstructure was revealed by fracturing the pellets. The morphologies of specimens calcined at 750 °C and 850 °C are shown in Fig. 6a and b. SEM images (6a and b) show that the calcined samples consist of very small particles with average grain size of 150 ± 50 nm and 200 ± 50 nm for samples calcined at 750 °C and 850 °C respectively. SEM images of the samples sintered at 1050 °C, 1350 °C and 1450 °C are shown in Fig. 7a–c. The specimen sintered at 1050 °C (Fig. 7a) exhibits small equi-axed particles with average size of about 400 ± 50 nm, although larger agglomerates (i.e., secondary particles) are also seen. Anyway, substantial grain growth is not recorded at this sintering temperature. Pronounced grain growth is seen at the sintering temperature of 1350 °C (Fig. 7b) and 1450 °C (Fig. 7c). The specimen sintered at 1350 °C (Fig. 7b) composes of uniform coarse structure with a well-clear crystalline microstructure having very small numbers of spherical small particles. The average grain size for the specimen sintered at 1350 °C was about 5 ± 2 μm. An average grain size of 8 ± 2 μm was obtained at 1450 °C (Fig. 7c). Structural parameters of $MgFe_2O_4$ specimens at different temperatures are summarized in Table 2. It can be noticed that $MgFe_2O_4$ specimen sintered at 1050 °C has lower relative density (79.5%) as compared to specimens sintered at 1350 °C (81%) and 1450 °C (84.2%). EDX analysis of the $MgFe_2O_4$ sample sintered at 1450 °C was performed for elemental analysis. In the EDX spectra (Fig.8) no impurity element is seen, except Mg, Fe and O. The atomic ratio of Mg and Fe is approximately 1:2.

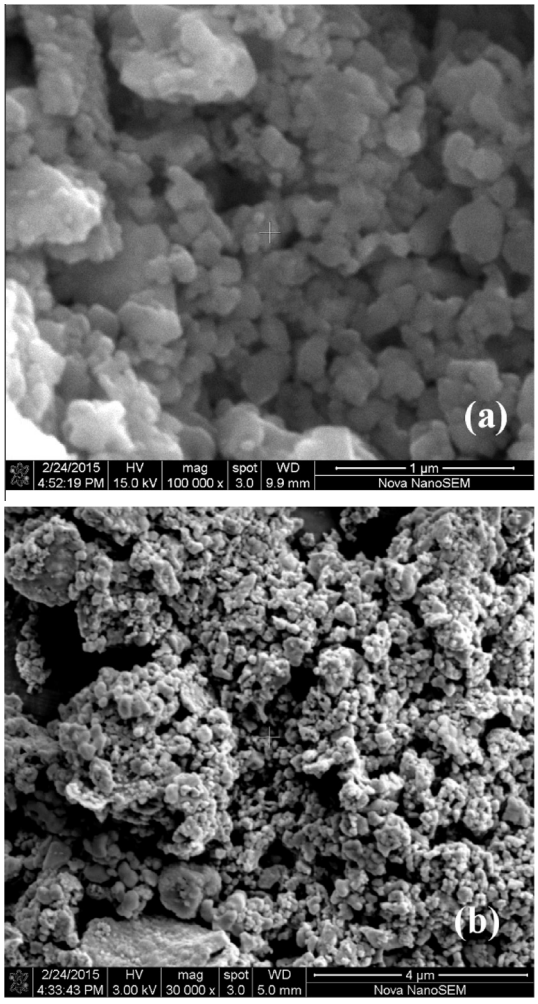

Figure 6 SEM images $MgFe_2O_4$ specimens calcined at (a) 750 °C and (b) 850 °C for 4 h.

3.5. UV–visible analysis

Fig. 9 shows UV–vis absorption spectrum of $MgFe_2O_4$ specimen calcined at 850 °C as a function of wavelength in nanometer. The characteristic bands around 300–400 nm (Fig. 9a), are pronounced in the optical absorption spectrum of magnesium ferrite spinel. These bands are due to Fe^{3+} ions in the octahedral coordination [57]. The absorption cut-off wavelength was 571.24 nm, suggesting that $MgFe_2O_4$ absorbs visible light in the wavelength range 500–650 nm. Band gap energy estimated by Tauc's plot (Fig. 9b) is about 2.175 eV. The following relationship has been used [58,59]:

$$\alpha = \frac{A}{h\nu}(h\nu - E_g)^{1/2} \quad (1)$$

where α is the absorption coefficient, $h\nu$ the photon energy, E_g the band gap energy and A is constant depending on the type of transition. Eq. (1), for any energy can be rearranged and written in the form:

$$(\alpha h\nu)^2 = A^2(h\nu - E_g) \quad (2)$$

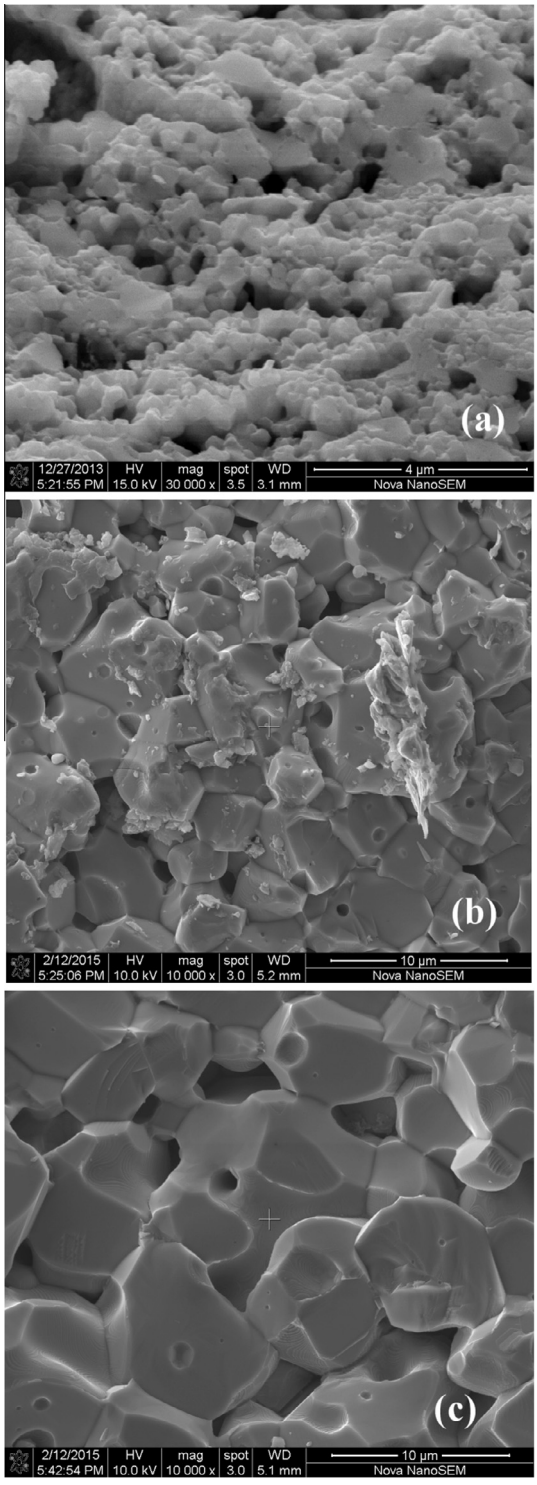

Figure 7 SEM images $MgFe_2O_4$ specimens: sintered at: (a) 1050 °C, (b) 1350 °C, and (c) 1450 °C for 4 h.

From Eq. (2), it is clear when $\alpha h\nu = 0$ then $E_g = h\nu$. The band gap energy was determined by plotting $(\alpha h\nu)^2$ against $h\nu$ and finding the intercept on the $h\nu$ axis by extrapolating the plot to $(\alpha h\nu)^2 = 0$ as shown in Fig. 9b (inset fig.). The band gap energy was determined from the intercept of the straight

Table 2 Structural parameters of $MgFe_2O_4$ specimens.

Sr. #	Specimens temperature (°C)	Lattice constant (Å)	Density (g/cm^3)	Particle size	Relative density (%)	Porosity (%)
1	Calcined 750	8.38341	–	150 ± 50 nm	–	–
2	Calcined 850	8.37642	–	200 ± 50 nm	–	–
3	Sintered 1050	8.36946	3.58	400 ± 50 nm	79.5	20.5
4	Sintered 1350	8.35903	3.61	5 ± 2 μm	81.0	19.0
5	Sintered 1450	8.36893	3.79	8 ± 2 μm	84.2	15.8

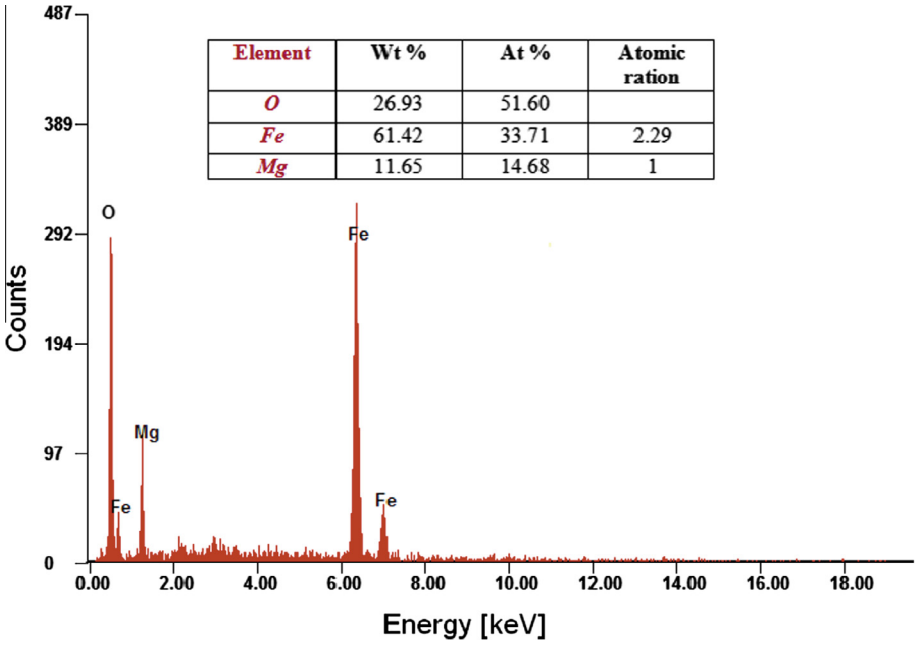

Figure 8 EDX curve and elemental composition (inset table) of $MgFe_2O_4$ pellet specimen sintered at 1450 °C for 4 h.

line at $\alpha = 0$, which was found to be 2.175 eV and close to the literature values. The reported band gap energy for $MgFe_2O_4$ is in the range 2.0–2.2 eV [53,60,61].

3.6. Mössbauer analysis

3.6.1. Mössbauer analysis of calcined powders

Mössbauer spectra of magnesium ferrite powder calcined at 750 °C and 850 °C are shown in Fig. 10. After a number of trials spectrum of the sample calcined at 750 °C (Fig. 10a) was very well fitted with four subspectra, three sextets (six-line spectrum) and a doublet (two-line spectrum). Ferrites have a spinel structure having two magnetic sublattices in which cations occupy tetrahedral A site and octahedral B sites. This differentiation can be done on the basis of isomer shift (δ) values; A-site has less δ than that of B-site. Therefore, one subspectrum is for tetrahedral site and three subspectra are for octahedral sites. In case of bulk ferrite the Mössbauer spectrum generally consists of two components; one for A-site and one for B-site. In magnetic ferrites the presence of quadrupole doublet indicates the presence of superparamagnetic material. Moreover, the presence of broad sextet (Fig. 10a) with very large line width (Γ = 2.01 mm/s) and large relative area (63%) correspond to $MgFe_2O_4$ superparamagnetic material. However other two sextets were due to the well developed structure of Ferrite (Fe^{3+}) segregated in various Fe sites. The cation distribution derived from the Mössbauer parameters of powder calcined at 750 °C can be given as $(Mg_{0.74}Fe_{0.26})[Mg_{0.13}Fe_{0.87}]_2O_4$. The presence of Mg cations at both A and B-sites indicate that Mg ferrite has a mixed spinel structure. The Mössbauer spectrum of the sample calcined at 850 °C (Fig. 10b), comprises three sextets and no doublet indicating the increase in the particle size as compared to the sample calcined at 750 °C. The cations distribution at this temperature was estimated as $(Mg_{0.54}Fe_{0.46})[Mg_{0.23}Fe_{0.77}]_2O_4$. The detail Mössbauer parameters are given Table 3.

3.6.2. Mössbauer analysis of sintered pellets

Fig. 11 shows the room temperature Mössbauer spectra of magnesium ferrite samples sintered at 1350 °C and 1450 °C for 4 h. One subspectrum is fitted for tetrahedral site (A-site) and one for octahedral site (B-site). In most of spinel ferrites the internal magnetic field (H_{eff}) is larger at B-site than that of A-site due to the dipolar field originating from the deviation from cubic symmetry and covalent nature of the tetrahedral bond [62–64]. Cationic distribution can be estimated from Mössbauer parameters given in Table 4 as $(Mg_{0.6}Fe_{0.4})[Mg_{0.2}Fe_{0.8}]_2O_4$ for the sample sintered at 1350 °C and $(Mg_{0.58}Fe_{0.42})[Mg_{0.21}Fe_{0.79}]_2O_4$ for the sample sintered at 1450 °C. There is not very much difference between the parameters of two

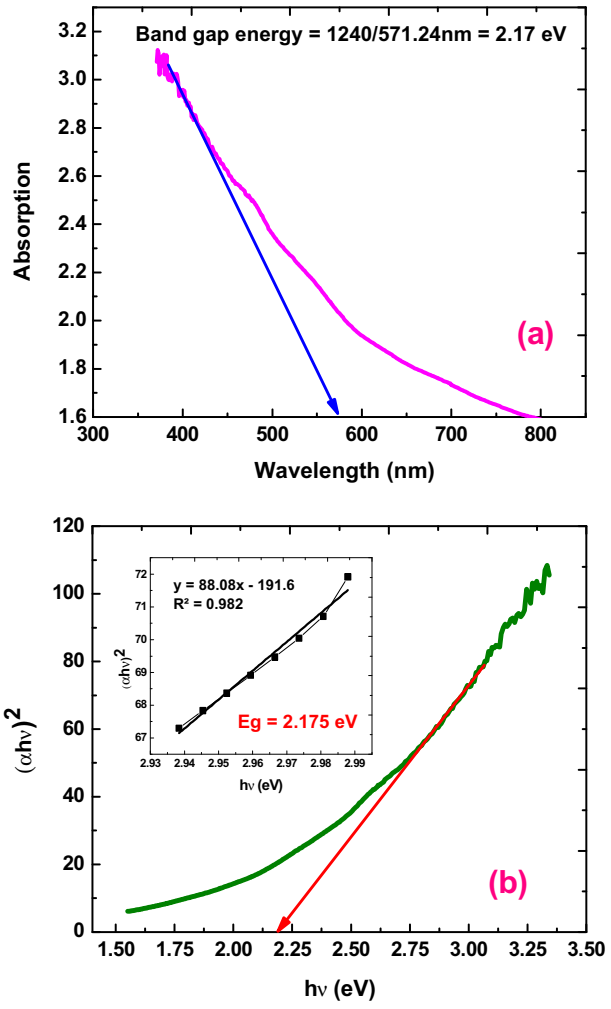

Figure 9 UV–visible absorption properties of $MgFe_2O_4$ specimen calcined at 850 °C: (a) UV–visible, and (b) Tauc's plot.

samples, however internal magnetic field decrease with the increase in temperature. By increasing the sintering temperature, more refined sextets (Fig. 11) were observed due to proper well defined crystal structures of $MgFe_2O_4$ obtained after sintering and also observed in SEM images (Fig.7b and c).

3.7. Impedance analysis

Fig. 12 shows impedance plane plots of $MgFe_2O_4$ specimens sintered at high temperatures 1350 °C and 1450 °C. The intersection of the semicircles at low frequencies (right hand side) give the total resistance of the $MgFe_2O_4$ sample sintered at 1350 °C and 1450 °C temperatures. Fig. 12a shows the appearance of two semi circle arcs in the impedance plane plots and the third semicircle arcs appearing at high frequencies are plotted in the inset, indicated by an arrow. The appearance of three semi circle arcs indicated the existence of at least three types of relaxation phenomena with different relaxation times ($\tau = RC$) where, τ, R, and C are the relaxation time, resistance and capacitance of the charge carriers, respectively. The change in the diameter of the arc of impedance plane plots of these two sintered samples can be explained on the basis

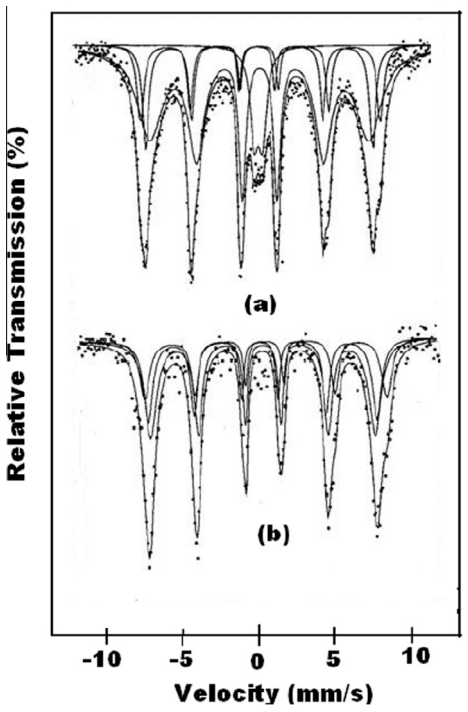

Figure 10 Mössbauer spectra of $MgFe_2O_4$ specimens calcined at (a) 750 °C, and (b) 850 °C for 4 h.

of three electro-active regions. Depending upon the geometric capacitance values, three electro active regions in the impedance plane plots were named as electrode, grain boundary and bulk associated with low, intermediate and high frequency arcs, respectively. To understand the effect of grain growth on the electrical properties of $MgFe_2O_4$ sintered specimens, an equivalent circuit model $(R_1Q_1)(R_2Q_2)(R_3Q_3)$ was employed. Where, R was used for resistance and Q for constant phase element, respectively. The suffix 1, 2 and 3 was used for grain, grain boundary and electrode effect, respectively. The constant phase element Q was used for non ideal capacitor. The deviation from ideal behavior was estimated by a parameter n, such that $C = R^{(1-n)/n}\ Q^{1/n}$, (for pure capacitor value $n = 1$). Equivalent circuit fitted parameters were tabulated in Table 5. The values of resistance of grain, grain boundary and electrode effect decreases with the sintering temperatures. These results are in accordance with our SEM analysis portion where grain growth is shown with an increase in the sintering temperature of the sample.

The log–log plot of real part of conductivity (σ') for $MgFe_2O_4$ sample sintered at 1350 °C and 1450 °C temperatures is shown in Fig. 12b. The frequency at which the slope of the conductivity changes is known as hopping frequency. The ac conductivity as a function of frequency for these two sintered samples enables us to correlate the electrical response to the different electro-active regions. A visible change in the frequency independent region (dc conductivity) can be viewed at low frequency side followed by intermediate frequency region (500–75 kHz) and these two frequency region represents electrode effect and grain boundary regions. The change in dc conductivity was associated with the drift mobility of the charge carriers. At higher frequency side conductivity curve seems to merge with each other for both sintered samples.

Please cite this article in press as: S.K. Durrani et al., Structural, impedance and Mössbauer studies of magnesium ferrite synthesized via sol–gel auto-combustion process, Journal of Saudi Chemical Society (2016), http://dx.doi.org/10.1016/j.jscs.2015.12.006

Table 3 Mössbauer parameters of $MgFe_2O_4$ calcined specimens.

Calcined temperature (°C)	Spectrum	H_{eff} (kOe)	Δ (mm s^{-1})	δ (mm s^{-1})	Γ (mm s^{-1})	Relative area (%)
750	Sextet 1	493 (±5)	0.04 (±0.002)	0.36 (±0.05)	0.50 (±0.05)	13 (±0.5)
	Sextet 2	467 (±4)	0.12 (±0.005)	0.24 (±0.03)	0.50 (±0.04)	15 (±1.0)
	Sextet 3	452 (±5)	-0.05 (±0.001)	0.34 (±0.02)	2.01 (0.015)	63 (±3.0)
	Doublet 1	–	0.55 (±0.05)	0.27 (±0.04)	0.65 (±0.04)	9 (±1.0)
850	Sextet 1	497 (±3)	0.04 (±0.001)	0.47 (±0.02)	0.78 (±0.05)	23 (±3.0)
	Sextet 2	470 (±2)	0.15 (±0.04)	0.21 (±0.02)	0.73 (±0.04)	30 (±5)
	Sextet 3	460 (±3)	−0.04 (0.002)	0.31 (0.03)	0.95 (±0.03)	47 (±1.0)

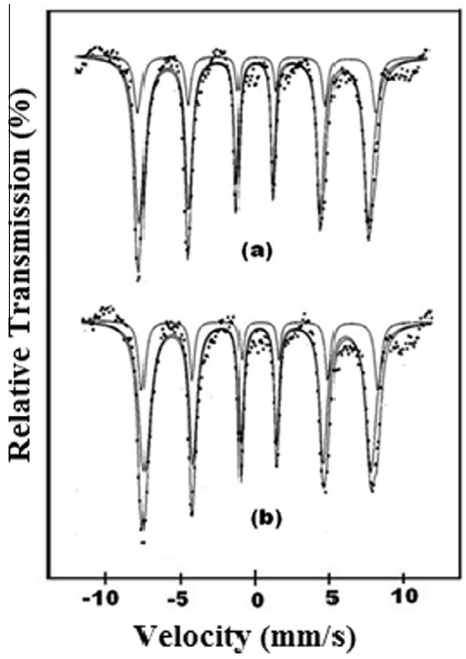

Figure 11 Mössbauer spectra of $MgFe_2O_4$ pellets sintered at: (a) 1350 °C, and (b) 1450 °C for 4 h.

Fig. 12c shows frequency dependent real part of dielectric constant (ε') for the investigated samples sintered at 1350 °C and 1450 °C. The trend of graphs is in accordance with impedance and conductivity results discussed above. Dispersion below 80 Hz shows high values of dielectric constant and was suggested to be due to the interfacial polarization. In the intermediate frequency region (500–75 kHz), grain boundary contributes mainly to the dielectric constant values and the sintering effect results in the grain growth and a decrease of grain boundaries results in lowering of impedance and dielectric values. At higher frequencies ($> 10^5$ Hz), relatively independent dielectric constant values were attributed to the atomic and electronic polarizations.

4. Conclusions

Magnesium iron ferrite ($MgFe_2O_4$) soft magnetic material was successfully synthesized by sol–gel auto-combustion method. Single cubic phase of $MgFe_2O_4$ was achieved after calcination at 850 °C for 4 h. Rietveld refined X-ray diffraction pattern confirmed the formation of pure phase $MgFe_2O_4$ space group of Fd3m (cubic spinel) with a parameter of $a = 8.3931$ Å. UV–visible examination of $MgFe_2O_4$ powder calcined at 850 °C reveals an optical band gap of 2.17 eV. FTIR spectra of the calcined powder showed two absorption bands at around 535 cm^{-1} and 410 cm^{-1} due to stretching vibrations of tetrahedral and octahedral group complexes of Fe^{3+}–O^{2-} bands in $MgFe_2O_4$ ferrite. Shrinkage characteristic was measured by dilatometry and suitable sintering temperature was found to be above 900 °C. On the basis of these findings $MgFe_2O_4$ dense pellets were formed by sintering at 1050 °C, 1350 °C and 1450 °C for 4 h. Crystallinity and grain size of the products increases with the increase in sintering temperatures. Mössbauer spectrum of the calcined magnetic ferrites showed

Table 4 Mössbauer parameters of $MgFe_2O_4$ sintered specimens.

Sintering temperature (°C)	Spectrum	Site	H_{eff} (kOe)	Δ (mm s^{-1})	δ (mm s^{-1})	Γ (mm s^{-1})	Relative area (%)
1350	Sextet 1	B	500 (±4)	0.00 (±0.00)	0.40 (±0.03)	0.55 (±0.05)	20 (±2)
	Sextet 2	A	480 (±5)	−0.04 (±0.01)	0.26 (±0.02)	0.76 (±0.07)	80 (±6)
1450	Sextet 1	B	494 (±6)	−0.02 (±0.005)	0.37 (±0.04)	0.48 (±0.03)	21 (±3)
	Sextet 2	A	474 (±5)	0.067 (±0.02)	0.26 (±0.01)	0.85 (±0.06)	79 (±5)

Table 5 Impedance analysis of $MgFe_2O_4$ sintered specimens.

Sintering temperature (°C)	R_1 (Ωs)	C.P.E_1	n_1	R_2 (Ωs)	C_2 (Farads)	n_2	R_3 (Ωs)	C.P.E_3	n_3
1350	98,343	2.36×10^{-9}	0.61	5.41×10^{6}	7.5×10^{-10}	1.0	3.39×10^{7}	2.35×10^{-9}	0.87
1450	76,474	4.89×10^{-9}	0.56	5.41×10^{6}	4.4×10^{-10}	1.0	1.64×10^{7}	2.77×10^{-9}	0.82

Please cite this article in press as: S.K. Durrani et al., Structural, impedance and Mössbauer studies of magnesium ferrite synthesized via sol–gel auto-combustion process, Journal of Saudi Chemical Society (2016), http://dx.doi.org/10.1016/j.jscs.2015.12.006

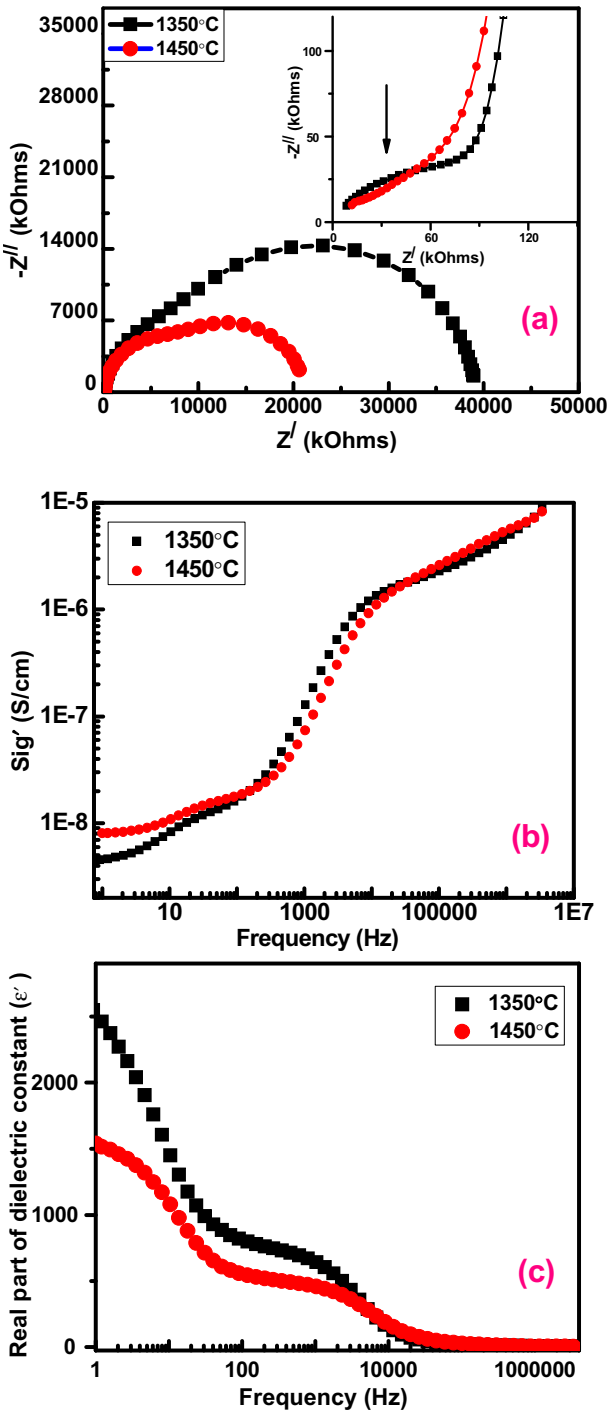

Figure 12 (a) Impedance analysis of $MgFe_2O_4$ specimens sintered at 1350 °C and 1450 °C for 4 h. Inset shows semicircles at high frequencies, (b) log–log conductivity plots with frequencies, and (c) variations of dielectric constants with frequencies.

quadrupole doublet at 750 °C indicating the presence of superparamagnetism behavior in the material whereas, this doublet disappears at 850 °C showing the increase in the particle size. Sintered specimens (1350 °C and 1450 °C) showed well define sextets related to Fe^{3+} at the tetrahedral (A) and the octahedral (B) sites. Mössbauer parameters also showed that magnesium ferrite had mix spinel structure. Impedance spectroscopy conferred decrease in the resistance values with temperature of different electro active regions. At higher frequencies, independent dielectric constant values were attributed to the atomic and electronic polarizations.

Acknowledgements

One of the authors (Sumaira Naz) acknowledges the financial support of the Higher Education Commission (HEC), Pakistan through the 'Indigenous Ph.D. fellowship for 5000 scholars' Phase-II, Batch-I, 2012, scholarship scheme in Science and Technology.

References

[1] I. Safarik, M. Safarikova, Magnetic nanoparticles and bioscience, in: H. Hofmann, Z. Rahman, U. Schubert (Eds.), Nanostructured Materials, Springer Verlag, Wien, 2002, pp. 1–23.
[2] Q. Xu, Y. Wei, Y. Liu, X. Ji, I. Yang, M. Gu, Preparation of Mg/Fe spinel ferrite nanoparticles from Mg/Fe-LDH microcrystallites under mild conditions, Solid State Sci. 11 (2009) 472–478.
[3] D.S. Mathew, R.S. Juang, An overview of the structure and magnetism of spinel ferrite nanoparticles and their synthesis in microemulsions, Chem. Eng. J. 129 (2007) 51–65.
[4] R.A. Candeiaa, M.I.B. Bernardib, E. Longoc, I.M.G. Santosa, A.G. Souza, Synthesis and characterization of spinel pigment $CaFe_2O_4$ obtained by the polymeric precursor method, Mater. Lett. 58 (2001) 569–572.
[5] A.C.F.M. Costa, A.M.D. Leite, H.S. Ferreira, R.H.G.A. Kiminami, S. Cava, L. Gama, Brown pigment of the nanopowder spinel ferrite prepared by combustion reaction, J. Eur. Ceram. Soc. 28 (2008) 2033–2037.
[6] X.Y. Wang, G. Yang, Z. Zhang, L. Yan, J. Meng, Synthesis of strong-magnetic nanosized black pigment $Zn_xFe_{(3-x)}O_4$, Dyes Pigm. 74 (2007) 269–272.
[7] C. Sun, J.S.H. Lee, M. Zhang, Magnetic nanoparticles in MR imaging and drug deliver, Adv. Drug Deliv. Rev. 60 (2008) 1252–1265.
[8] N.L. Rosi, C.A. Mirkin, Nanostructures in biodiagnostics, Chem. Rev. 105 (2005) 1547–1562.
[9] R.S. Molday, D. Mackenzie, Immunospecific ferromagnetic iron-dextran reagents for the labeling and magnetic separation of cells, J. Immun. Methods 52 (1982) 353–367.
[10] J.H. Lee, Y.M. Huh, Y.W. Jun, J.W. Seo, J.T. Jang, H.T. Song, S. Kim, E.J. Cho, H.G. Yoon, J.S. Suh, J. Cheon, Artificially engineered magnetic nanoparticles for ultra-sensitive molecular imaging, Nat. Med. 13 (2007) 95–99.
[11] A.M. Schmidt, Thermoresponsive magnetic colloids, Colloid Polym. Sci. 285 (2007) 953–966.
[12] N.K. Prasad, K. Rathinasamy, D. Panda, D. Bahadur, Mechanism of cell death induced by magnetic hyperthermia with nanoparticles of γ-$Mn_xFe_{2-x}O_3$ synthesized by a single step process, J. Mater. Chem. 17 (2007) 5042–5051.
[13] Y. Kinemuchi, K. Ishizaka, H. Suematsu, W. Jiang, K. Yatsui, Magnetic properties of nanosize $NiFe_2O_4$ particles synthesized by pulsed wire discharge, Thin Solid Films 407 (2002) 109–113.
[14] R.J. Willey, P. Noirclerc, G. Busca, Preparation and characterization of magnesium chromite and magnesium ferrite aerogels, Chem. Eng. Commun. 123 (1993) 1–16.
[15] S.A. Oliver, R.J. Willey, H.H. Hamdeh, G. Oliveri, G. Busca, Magnetic properties of partially-inverted zinc ferrite aerogel powders, Scr. Meth. Mater. 33 (1995) 1695–1701.
[16] K.S. Rane, V.M.S. Verenkar, P.Y. Sawant, Dielectric behaviour of $MgFe_2O_4$ prepared from chemically beneficiated iron ore rejects, Bull. Mater. Sci. 24 (2001) 323–330.

[17] A. Goldman, Modern Ferrite Technology, Springer Science Business Media Inc., New York, 2006.
[18] G. Busca, E. Finocchio, V. Lorenzelli, M. Trombetta, S.A. Rossini, IR study of alkene allylic activation on magnesium ferrite and alumina catalysts, J. Chem. Soc. Faraday Trans. 92 (1996) 4687–4693.
[19] Y. Shimizu, H. Arai, T. Seiyama, Theoretical studies on the impedance-humidity characteristics of ceramic humidity sensors, Sens. Actuators 7 (1985) 11–22.
[20] K. Seki, J.I. Shida, H. Murakami, Use of a temperature-sensitive ferrite for temperature/humidity measurements, IEE Trans. Instrum. Meas. 37 (1988) 468–470.
[21] L.G.J. de Haart, G. Blasse, Photoelectrochemical properties of ferrites with the spinel St state ionics, Solid State Ionics 16 (1985) 137–139.
[22] Y. Huang, Y. Tang, J. Wang, Q. Chen, Synthesis of $MgFe_2O_4$ nanocrystallites under mild conditions materials chemistry and physics, Mater. Chem. Phys. 97 (2006) 394–397.
[23] R. Dom, R. Subasri, K. Radha, P.H. Borse, Synthesis of solar active nanocrystalline ferrite, MFe_2O_4 (M: Ca, Zn, Mg) photocatalyst by microwave irradiation, Solid State Commun. 151 (2011) 470–473.
[24] Y. Watanabe, K. Sato, S. Yukumi, M. Yoshida, Y. Yamamoto, T. Doi, H. Sugishita, T. Naohara, T. Maehara, H. Aono, K. Kawachi, Development of a second radiofrequency ablation using sintered $MgFe_2O_4$ needles and alternating magnetic field for human cancer therapy, Bio-Med. Mater. Eng. 19 (2009) 101–110.
[25] S. Yukumi, Y. Watanabe, A. Horiuchi, T. Doi, K. Sato, M. Yoshida, T. Maehara, H. Aono, T. Naohara, K. Kawachi, Feasibility of induction heating using a sintered $MgFe_2O_4$ needle for minimally invasive breast cancer therapy, Anticancer Res. 28 (2008) 69–74.
[26] P. Ravindranathan, K.C. Patil, Novel solid solution precursor method for the preparation of ultrafine Ni–Zn ferrites, J. Mater. Sci. 22 (1987) 3261–3264.
[27] T. Žák, V. Ćosović, A. Ćosović, B. David, N. Talijan, D. Živković, Formation of magnetic microstructure of the nanosized $NiFe_2O_4$ synthesized via solid-state reaction, Sci. Sintering 44 (2012) 103–112.
[28] V. Sepelak, D. Baabe, D. Mienert, Evolution of structure and magnetic properties with annealing temperature in nanoscale high-energy-milled nickel ferrite, J. Magn. Magn. Mater. 257 (2003) 377–386.
[29] Z. Zhang, Y. Liu, G. Yao, G. Zu, Y. Hao, Synthesis and characterization of $NiFe_2O_4$ nanoparticles via solid-state reaction, Int. J. Appl. Ceram. Technol. 10 (2013) 142–149.
[30] P.L. Leng, M.G. Naseri, E. Saion, A.H. Shaari, M.A. Kamaruddin, Synthesis and characterization of Ni–Zn ferrite nanoparticles ($Ni_{0.25}Zn_{0.75}Fe_2O_4$) by thermal treatment method, Adv. Nanopart. 2 (2013) 378–383.
[31] M. Pavlovic, C. Jovalekic, A.S. Nikolic, D. Manojlovic, N. Sojic, Mechanochemical synthesis of stoichiometric $MgFe_2O_4$ spinel, J. Mater. Sci. 20 (2009) 782–787.
[32] P. Holec, J. Plocek, D. Niznansky, J.P. Vejpravova, Preparation of $MgFe_2O_4$ nanoparticles by microemulsion method and their characterization, J. Sol-Gel. Sci. Technol. 51 (2009) 301–305.
[33] J. Fang, N. Shama, L.D. Tung, E.Y. Shin, C.J. O'Connor, K.L. Stokers, G.l. Caruntu, J.B. Wiley, L. Spinu, J. Tang, Ultrafine $NiFe_2O_4$ powder fabricated from reverse microemulsion process, J. Appl. Phys. 93 (2003) 7483–7486.
[34] K.V.P.M. Shafi, Y. Koltypin, A. Gedanken, R. Prozorov, J. Balogh, J. Lendvai, I. Felner, Sonochemical preparation of nanosized amorphous $NiFe_2O_4$ particles, J. Phys. Chem. B 101 (1997) 6409–6414.
[35] S.J. Haralkar, R.H. Kadam, S.S. More, S.E. Shirsath, M.L. Mane, Swati Patil, D.R. Mane, Substitutional effect of Cr^{3+} ions on the properties of Mg–Zn ferrite nanoparticles, Physica B 407 (2012) 4338–4346.
[36] M.V. Chaudhari, S.E. Shirsath, A.B. Kadam, R.H. Kadam, S.B. Shelke, D.R. Mane, Site occupancies of Co–Mg–Cr–Fe ions and their impact on the properties of $Co_{0.5}Mg_{0.5}$ $Cr_xFe_{2-x}O_4$, J. Alloys Compd. 552 (2013) 443–450.
[37] E.C. Sousa, C.R. Alves, R. Aquino, M.H. Sousa, G.F. Goya, H. R. Rechenberg, F.A. Tourinho, J. Depeyrot, Experimental evidence of surface effects in the magnetic dynamics behavior of ferrite nanoparticles, J. Magn. Magn. Mater. 289 (2005) 118–121.
[38] A. Chaudhuri, S. Mitra, M. Mandal, K. Mandal, Nanostructured bismuth ferrites synthesized by solvothermal process, J. Alloys Compd. 491 (2010) 703–706.
[39] S.K. Durrani, S. Naz, M. Nadeem, E. Ahmed, M. Siddique, Thermal, structural analysis, Mössbauer and impedance study of copper nickel ferrite nanoparticles synthesized via Tween80-assisted hydrothermal process, J. Therm. Anal. Calorim. 119 (2015) 253–263.
[40] L. Zhao, H. Zhang, Y. Xing, S. Song, S. Yu, W. Shi, X. Guo, J. Yang, Y. Lei, Studies on the magnetism of cobalt ferrite nanocrystals synthesized by hydrothermal method, J. Solid State Chem. 18 (2008) 245–252.
[41] S.K. Durrani, S. Naz, K. Hayat, Thermal analysis and phase evolution of nonocrystalline perovskite oxide materials synthesized via hydrothermal and self-combustion methods, J. Therm. Anal. Calorim. 115 (2014) 1371–1380.
[42] S. Naz, S.K. Durrani, M. Mazhar, M. Nadeem, Hydrothermal synthesis, structural and impedance studies of nanocrystalline zinc chromite spinel oxide material, J. Saudi Chem. Soc. (2015), http://dx.doi.org/10.1016/j.jscs.2014.12.007.
[43] Z. Fenlian, M. Yongqing, M. Qian, X. Yuanfeng, D. Zhenxiang, Z. Ganhong, W. Mingzai, L. Guang, Magnetic and impedance properties of nanocomposite $CoFe_2O_4/Co_{0.7}Fe_{0.3}$ and single-phase $CoFe_2O_4$ prepared via a one-step hydrothermal synthesis, J. Am. Ceram. Soc. 96 (2013) 3100–3107.
[44] S.K. Durrani, S.Z. Hussain, K. Saeed, Y. Khan, M. Arif, N. Ahmed, Hydrothermal synthesis and characterization of nanosized transition metal chromite spinels, Turk. J. Chem. 36 (2012) 111–120.
[45] S.K. Durrani, S. Naz, M. Nadeem, A.A. Khan, Thermal, structural, and impedance analysis of nanocrystalline magnesium chromite spinel synthesized via hydrothermal process, J. Therm. Anal. Calorim. 116 (2014) 309–320.
[46] A. Varma, A.S. Rogachev, A.S. Mukasyan, S. Hwang, Combustion synthesis of advanced materials: principles and applications, Adv. Chem. Eng. 24 (1998) 79–226.
[47] R.Q. Chu, Z.J. Xu, Synthesis of mixed-conducting oxide $SrFeCo_{0.5}Oy$ powder by auto-combustion of citrate–nitrate gel, J. Electroceram. 21 (2008) 778–781.
[48] S. Naz, S.K. Durrani, A.H. Qureshi, M.A. Hussain, N. Hussain, Nanosized bismuth titanate ($Bi_4Ti_3O_{12}$) system drive through auto-combustion process by using suspension titania (TiO_2), J. Therm. Anal. Calorim. 114 (2013) 719–723.
[49] A. Sutka, G. Mezinskis, G. Strikis, A. Siskin, Gas sensitivity of stoichiometric and excess-iron Ni–Zn ferrite prepared by sol–gel auto combustion, Energetika 58 (2012) 166–172.
[50] M.B. Kakade, S. Ramanathan, G.P. Kothyiyal, Nano-alumina by gel combustion, its thermal characterization and slurry-based coating on stainless steel surface, J. Therm. Anal. Calorim. 112 (2013) 133–140.
[51] Gerhard Groβe MOS-90, Version 2.2, Manual and Program Documentation second ed., March 1992.
[52] Köferstein Roberto, T. Walther, D. Hesse, S.G. Ebbinghaus, Preparation and characterization of nanosized magnesium ferrite powders by a starch-gel process and corresponding ceramics, J. Mater. Sci. 48 (2013) 6509–6518.

Please cite this article in press as: S.K. Durrani et al., Structural, impedance and Mössbauer studies of magnesium ferrite synthesized via sol–gel auto-combustion process, Journal of Saudi Chemical Society (2016), http://dx.doi.org/10.1016/j.jscs.2015.12.006

[53] A.B. Gadkari, T.J. Shinde, P.N. Vasambekar, Structural and magnetic properties of nanocrystalline Mg–Cd ferrites prepared by oxalate co-precipitation method, J. Mater. Sci. Mater. Electron. 21 (2010) 96–103.
[54] W.F. McClune (Ed.), Powder Diffraction File, Inorganic Phases, International Centre for Diffraction, Swarthmore, PA, 1989.
[55] H.M. Rietveld, A profile refinement method for nuclear and magnetic structures, J. Appl. Crystallogr. 2 (1969) 65–71.
[56] M. Gaudon, N. Pailhe, A. Wattiaux, A. Demourgues, Structural defects in AFe_2O_4 (A = Zn, Mg) spinels, Mater. Res. Bull. 44 (2009) 479–484.
[57] J. Tauc, R. Grigorovici, A. Vancu, Optical properties and electronic structure of amorphous germanium, Phys. State Solid 15 (1966) 627–637.
[58] L. Zhang, J.F. Guang, F. Zhao, Z.Z. Gong, First-principles study of the structural, mechanical and electronic properties of ZnX_2O_4 (X = Al, Cr and Ga), Chin. Phys. B 20 (2011) 047102–047107.
[59] B.D. Hosteman, J.W. Farley, A.L. Johnson, Spectroscopic study of the vibrational modes of magnesium nickel chromite, $Mg_xNi_{1-x}Cr_2O_4$, J. Phys. Chem. Solids 74 (2013) 985–990.
[60] G.D. Nipan, V.A. Ketsko, A.I. Stognij, A.V. Trukhanov, T.N. Koltsova, M.A. Kopeva, L.V. Elesina, N.T. Kuznetsov, Properties of Mg $(Fe_{1-x}Ga_x)_2O_{4+\delta}$ solid solutions in stable and metastable states, Inorg. Mater. 46 (2010) 429–433.
[61] H.G. Kim, P.H. Borse, J.S. Jang, E.D. Jeong, O.S. Jung, Y.J. Suh, J.S. Lee, Fabrication of $CaFe_2O_4/MgFe_2O_4$ bulk heterojunction for enhanced visible light photocatalysis, Chem. Commun. 39 (2009) 5889–5891.
[62] N.N. Greenwood, T.C. Gibb, Mössbauer Spectroscopy, Chapman & Hall, London, 1971, pp. 259.
[63] K.H. Rao, S.B. Raju, R.G. Mendiratta, J.P. Eymery, Hyperfine fields in Cr and In substituted Mn–Zn ferrites, Solid State Commun. 45 (1983) 919–923.
[64] R.E. Watson, A.J. Freeman, Origin of effective fields in magnetic materials, Phys. Rev. 123 (1961) 2027–2047.

Please cite this article in press as: S.K. Durrani et al., Structural, impedance and Mössbauer studies of magnesium ferrite synthesized via sol–gel auto-combustion process, Journal of Saudi Chemical Society (2016), http://dx.doi.org/10.1016/j.jscs.2015.12.006